Aust. J. Phys., 1987, **40**, 125–37

Excitation of Swift Heavy Ions in Foil Targets. III* Initial Populations of Rydberg States

H. J. Hay and P. B. Treacy

Department of Nuclear Physics, Research School of Physical Sciences,
Australian National University, G.P.O. Box 4, Canberra, A.C.T. 2601.

Abstract

Results are reviewed of experiments in which Rydberg states with high principal quantum numbers ($n \gtrsim 20$) are excited by foil targets in transmitted heavy ions. A uniform procedure is described for analysis of the decays downstream of such states using a Monte Carlo method. Previously observed X-ray decays of 130 MeV Br Rydberg ions into L vacancies are analysed and numerical populations of initially generated states are deduced. It is found that the initial states may be described as mainly statistical, i.e. all substates having equal weights, with 63% of initial ions in such states. Some X-ray lines are found to come from high-n ($\gtrsim 50$), low-l ($\lesssim 2$) states. There is evidence for an unknown post-foil mechanism feeding the 3s electron state.

1. Introduction

The work described here comprises an analysis of data by Hay *et al.* (1986; hereafter referred to as Part II), on the decay of Rydberg states with n values between 20 and 135, in 130 MeV Br ions excited in the beam–foil method by transmission through a 20 μg cm^{-2} carbon foil. That work has turned out to require a rather detailed treatment of the apparent production mechanisms involving four distinct L X-rays associated with ions having cores with L vacancies (ion charge states $\geqslant 25^+$). The decay of each of these X-rays was studied at distances between 8 and 190 mm downstream of the target. What is of obvious physical interest in such experiments is to explain how such relatively large ions, with r.m.s. orbital radii upwards of factors $n^2/Z = 16$ times the Bohr radius $0 \cdot 5$ Å, can emerge from a solid target with typical interatomic spacings of about 5 Å; also what initial population of n and l quantum numbers can account for the observed decays up to 10 ns later. In the present paper an attempt is made to invoke a unique population, with a view towards understanding its method of production.

Earlier work on the decay characteristics of high-n Rydberg states was carried out by Betz and co-workers (Betz *et al.* 1980, 1982; Rothermel *et al.* 1982), in studies of the decays of K vacancies. Evidence was given for the decays through yrast states, i.e. states of highest angular momentum $l = n-1$, with evidence that initial populations were fairly consistent with the n^{-3} law predicted from several capture mechanisms. In more recent work by Hay *et al.* (1983; hereafter Part I), Betz *et*

* Part II, *Aust. J. Phys.*, 1986, **39**, 15.

0004-9506/87/020125$02.00

al. (1983) and Dybdal *et al.* (1986) studies have been made of the target-thickness dependence of such populations. Such a dependence guarantees that no simple surface-excitation mechanism can be responsible. Recent work by Kanter *et al.* (1985) on the charge-state distributions of Rydberg ions with different target thicknesses provided a definite basis for studying the production mechanism. However, the present work is confined to initial populations based on the data of Part II, which were taken with a single target thickness.

In Section 2 we define the classes of population likely to be produced and the decays expected. The advantage here of utilising a multi-line L X-ray spectrum becomes apparent. Section 3 describes the expected decays in time from assumed initial populations, while Section 4 fits the intensities and decay curves of the four X-ray lines. The results (and some puzzles) are summarised in Section 5, with a sketch of possible transitions occurring. It should perhaps be pointed out here that considerable algebraic complexity is found to be necessary in Section 4 to establish the rather involved inter-relations among the cascades. However, the general ideas involved are evident from Fig. 1 and Table 1; the numerical details are documented in Sections 3 and 4.

2. Expected Populations and Decay Modes

Most of the experimental data referred to in Section 1 showed a very simple decay characteristic, namely a power-law intensity

$$I(t) = I_0\, t^{-\alpha}\,, \tag{1}$$

with α lying between $1\cdot 0$ and $1\cdot 5$.

In an important paper Hasse *et al.* (1979) showed that such a power-law decay follows as an asymptotic limit, if one assumes a population which depends on a given set of quantum numbers (n, l) according to

$$P_{nl} = B\, n^{-\beta} \tag{2}$$

and combines it with the Einstein decay probabilities A_{nl} as defined by Bethe and Salpeter (1957). For large n and l these have the form

$$A_{nl} = C\, n^{-\gamma}\,, \tag{3}$$

where $C = 10\cdot 7\, Z^4\ \mathrm{ns}^{-1}$ and Z is the ion core charge.

Hasse *et al.* took two cases of interest. For an yrast chain, characterised by the sequence of (n, l) values $(n, n-1)$, $(n-1, n-2), \ldots$, they predicted a decay law for any member of the sequence to be

$$I(n, t) = I(n, 0)\left(1 + \frac{\gamma+1}{n}\, A_{nl}\, t\right)^{-(\beta+\gamma)/(\gamma+1)}\,, \tag{4}$$

provided only that n is large enough to be treated in the mathematics as a continuous number. Cases of interest satisfy the condition

$$A_{nl}\,t \gg n/(\gamma+1), \tag{5}$$

so that the form of equation (1) is recovered, where

$$I_0 = C^{1-\alpha} B(\gamma+1)^{-\alpha} \quad \text{and} \quad \alpha = (\beta+\gamma)/(\gamma+1) \quad \text{(yrast decay)}. \tag{6}$$

The second case treated by Hasse *et al.* is that where many initial states $(n', l = 0)$ decay directly to a state $(n, l = 1)$—or more generally n' to n with $\Delta l = \pm 1$. In this case, provided that

$$A_{nl}\,t = n^{-\gamma} C t \gg 1, \tag{7}$$

one has again equation (1), where now

$$I_0 = C^{1-\alpha} B\Gamma(\alpha)/\gamma \quad \text{and} \quad \alpha = (\beta+\gamma-1)/\gamma \quad \text{(direct decay)}. \tag{8}$$

Notice that in both cases I_0 depends on the ionic charge Z as $Z^{4(1-\alpha)}$. For the cases to which equations (6) and (8) correspond, values of $\gamma = 5$ $(l = n-1)$ and $\gamma = 3$ $(l = 0)$ are required, as detailed by Bethe and Salpeter (cf. equation 11 below).

For the appropriate value to be used for β one must appeal to a production model. The most common (OBK) model predicts the n dependence of the population, summed over l, to be n^{-3}; a first Born approximation predicts this result as an asymptotic high-energy limit (Omidvar 1975). It is not obvious what l dependence should be assumed. The simplest choice consistent with equation (2) is

$$P_{nl} = B_{\mathrm{s}} \frac{2l+1}{n^2}\, n^{-\beta_{\mathrm{s}}}, \tag{9}$$

which evidently corresponds to a distribution with equal weights to the $2l+1$ substates of each l value. When summed over l, it yields

$$P_n = \sum_{l=0}^{n-1} P_{nl} = B_{\mathrm{s}}\, n^{-\beta_{\mathrm{s}}}. \tag{10}$$

Equation (9) is a statistical population which we now identify by the subscript s. A further restriction for which $\mathrm{d}P_n/\mathrm{d}E_n$ is constant (E_n is the term energy) leads to $\beta_{\mathrm{s}} = 3$; this we designate a *uniform* population. For such a population, the yrast members with $l = n-1$ have $\beta = 4$ and $\gamma = 5$ which, via equation (6), leads to a time decay index $\alpha = 3/2$. Similarly, the $l = 0$ members have $\beta = 5$ and $\gamma = 3$, whence $\alpha = 7/3$ (equation 8). This is an example of a general rule that lower-l cascades decay faster.

We note here that equations (6b) and (8b) show that the observation of a power-law decay (equation 1) requires a population index β (equation 2) which is constant and independent of n over the range of n observed. *In the following we take power-law decays as evidence for such populations.*

3. Interpretation of X-ray Decays

(a) Experimental Data to be Fitted

The results of the spectroscopic analysis of Part II may best be summarised by reference to the energy level diagram of Fig. 1. From well-known systematics of the mean substate energies based on the core $2s^2 2p^5$ (Bashkin and Stoner 1975, 1976, 1981), the X-rays observed by us were identified and designated as L_{A1}(3s–2p), L_{A23}(3d–2p), L_B(4f–2p) and L_C(nl–2p) with $n > 10$ and $l = 0$ or 2. These lines are named in increasing order of energy and decreasing order of intensity.

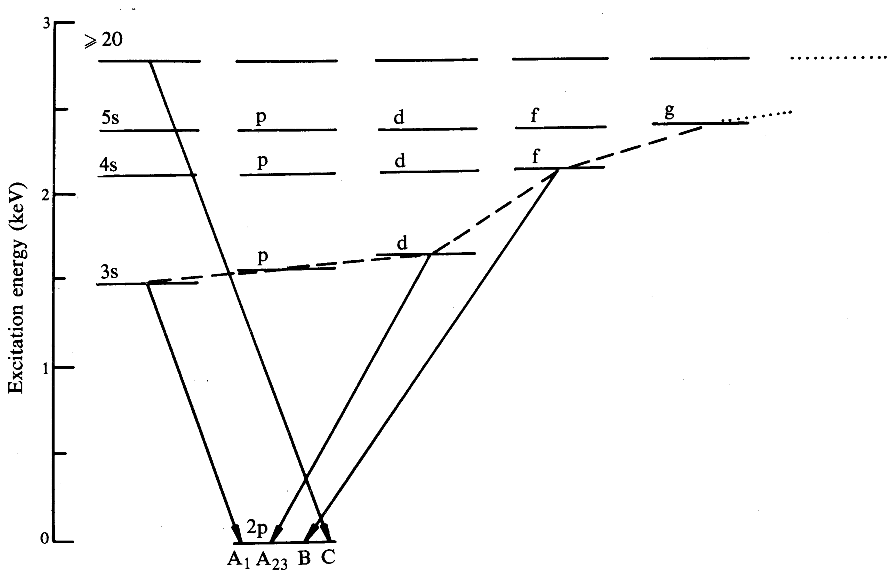

Fig. 1. Energy level diagram and decay scheme for Br ions with a single 2p vacancy. The four observed L X-ray lines labelled A_1, A_{23}, B and C are indicated by solid lines. The (unobserved) upper-yrast and trapped-yrast transitions are shown by dashed lines. For each n, the substate splittings are shown exaggerated, but the mean term energies are to scale.

Referring to the two analytic theories of decay chains in Section 2, we note that the energies of the lines L_{A23} and L_B, which have power-law decays with $\alpha = 1 \cdot 21$, correspond to the last electric dipole (E1) transition and an electric quadrupole (E2) crossover of the yrast chain, while L_C is a direct decay with $\alpha = 1 \cdot 46$. In Part II it was deduced, using equations (6) and (8), that the yrast and direct β values were $2 \cdot 26$ and $2 \cdot 38$. By comparing equations (2) and (9), it is seen that $l = n-1$ leads to $\beta = \beta_s + 1$ while $l = 0$ leads to $\beta = \beta_s + 2$. Hence, the two decay systems appear to correspond to β_s values of $1 \cdot 26$ and $0 \cdot 38$ respectively, and therefore do not belong to the same initial population.

The L_{A1} decay curve does not conform to a power-law form. It was noted in Part II that it could be represented as the sum of three components; namely, an apparently exponential decay at very short times, a power-law with the same index $\alpha = 1 \cdot 21$ as L_{A23} and L_B, and a constant which took effect at longer times. The interpretation of this complex decay is addressed in Sections 3b and 4b.

It should be mentioned here that the above description of the X-ray lines assumes one electron outside a single ionic core state. Cores with more than one excited electron shed the excess by Auger processes, while cores with L vacancies rearrange to their ground state configuration. In practice, this means that the observed X-rays are from cores with charges 27 and 26 whose measured relative intensities are in the ratio 0·22 (and <0·04 for 28 and above); all lines are thus in principle double. For a core with charge 27, the L_A X-ray energies are between 80 and 140 eV higher than for charge 26. These are included in the analysis of Section 4*b*.

Table 1. Modification of hydrogenic electric dipole lifetimes for an ion with a single 2p vacancy

Lifetimes τ and branch intensities are given for single-electron states above a single 2p vacancy. As discussed in Section 3*b*, allowance must be made for *n*d–2p transitions being blocked by 'trapping' of the *n*d states

Initial state	*n*d–2p blocked	τ	Final state	Branch (%)
3s		$6\tau_H$ (note A)	2p	100
3p		τ_{3ps} (note B)	3s	100
3d	No	$6\tau_H$	2p	100
3d	Yes	τ_{3dp} (note C)	3p	100
4s		$2\tau_H$	2p	18
			3p	82
4p		$25\tau_H$	3s	100
4d	No	$2\cdot6\tau_H$	2p	67
			3p	33
4d	Yes	$3\cdot9\tau_H$	3p	100
>4, s	No	$1\cdot5\tau_H$	2p	10
			3p	90
>4, p		$12\tau_H$	3s	50
			4s	50
>4, d	No	$2\tau_H$	2p	20
			3p	80
>4, d	Yes	$2\cdot5\tau_H$	3p	100
$n > l+1, l > 2$		τ_H	$l, l-1$	50
			$l+1, l-1$	50
$n = l+1, l > 2$		τ_H	$l, l-1$	100

[A] Hydrogenic lifetime (see Bethe and Salpeter 1957).
[B] Lifetime for the 3p–3s transition.
[C] Lifetime for the 3d–3p transition.

(b) Physical Assumptions: Monte Carlo Method

Because the analytical treatments leading to equations (6) and (8) do not include all the decays of significance among the levels of Fig. 1, it was decided to compute actual time-decay curves from given assumed populations using a Monte Carlo method. Certain assumptions had to be made as to the general forms of equations (2) and (3) to be used. Calculations were done with a statistical distribution, as well as for separate populations of the form (2) with $l = 0$, 1 and 2. Numerical forms for the lifetimes ($\tau = A_{nl}^{-1}$) were obtained from Bethe and Salpeter (Table 15 and equation

59.15). The n and l dependence of the hydrogenic lifetimes, which are predominantly electric dipole, are deduced to be

$$\tau_{\mathrm{H}}(n,0) = 2\,\frac{2n-3}{2n-5}\,n^3/Z^4\ \mathrm{ns}, \tag{11a}$$

$$\tau_{\mathrm{H}}(n, l>0) = 0\cdot0232(2l+1)^2\,n^3/Z^4\ \mathrm{ns}. \tag{11b}$$

The following extra conditions should be noted:

(i) Where there is a choice of final states for a decay, we took note of the general rules (Bethe and Salpeter; pp. 267–8) that decays in which n and l change in the same sense (both down) are strongly favoured and that the major intensity goes with the largest change of energy. For our calculations, these were simplified to a two-way branch (with $\Delta l = -1$ for $l > 0$) whereby 50% goes to the lowest available n and the remainder to $n+1$, i.e. the nearest integer to the intensity-weighted final energy.*

(ii) For cases where (for a true hydrogen ion) final states with $n = 1$ or 2 would be involved, total lifetimes were adjusted to allow for our case that all the former and all but one of the latter (in 25^+ ions) are filled. Examples of such restrictions are shown in Table 1. The most important consequence is that some of the d-to-p transitions are inhibited by the m_l selection rule ($\Delta m_l = 0, \pm1$). For an unpolarised beam of ions, it may be shown that a fraction $F = 0\cdot7$ are prevented, i.e. the yrast sequence is trapped at the 3d level. The dependence on trapping is shown in Table 1.

(iii) In addition to the E1 decays, a small E2 branch was included with the same conditions as (i) and (ii). The relative E2 : E1 intensity was not taken from any theory but was fitted to the observed $\mathrm{L_B} : \mathrm{L_{A23}}$ intensity ratio.

The consequences of these rules are that there are many more transitions occurring among the members of a statistical population than shown in Fig. 1. These include:

'Collapse' of (high-n, $l < n-1$) levels down to yrast levels in a few steps. For each l value, this proceeds according to equations (2), (8) and (11). Summation over n for each l shows that an instantaneous collapse would augment the original yrast population so as to nullify the one unit change of β_s, deduced in Section 3*a* where decay of non-yrast states was ignored. The effect of non-instantaneous collapse is a small change of $0\cdot125$ ($= 2\cdot260 - 2\cdot135$), as seen in the results of Table 2 in Section 4.

'Trapping' of some 3d levels in a fraction F of cases. Such levels decay via 3d–3p–3s transitions. These $\Delta n = 0$ transitions ($\tau_{3\mathrm{dp}}$ and $\tau_{3\mathrm{ps}}$ in Table 1) are slow, and the build-up with time of the 3s population from the yrast trap gives rise to the apparent exponential component of $\mathrm{L_{A1}}$ remarked on in Part II. At later times trapping manifests itself as a time delay and the decay approaches the same power-law as $\mathrm{L_{A23}}$. Since we have seen that 70% of yrast transitions are trapped, it follows that $\mathrm{L_{A1}}$(3s–2p) should be the dominant X-ray, as is indeed observed.

* Branching fractions between 20% and 80% were found to give substantially the same L X-ray intensities.

In addition, the rules now allow mixed contributions in such a way that, for example, L_C is no longer purely a 'direct' transition from high-n states with $l = 0$ or 2, but contains a contribution from the whole statistical distribution. Similarly, non-statistical low-l initial populations, mainly responsible for L_C, also give rise to some L_{A1}. Such effects must be included in interpreting the intensities of the separate L X-ray lines, as shown by the fitting procedure described in the next section.

4. Results of the Analysis

(a) Fitting Power-law Decays

The data to be fitted comprise the intensities, relative to the ion charge collected in a Faraday cup, of four X-ray lines, identified by energy and decay characteristics, at distances 8 to 190 mm (0·45 to 10·7 ns) downstream from the target. Fig. 5 of Part II shows that three of these, L_{A23}, L_B and L_C, have power-law decays while L_{A1} does not. As discussed in Section 3*a*, we associate L_{A1} and L_{A23} with the last transitions of an yrast chain (equation 6), L_B with an E2 branch from yrast, and L_C with low-l direct decays (equation 8).

In order to fit these to the Monte Carlo calculations, the following steps were taken:

(i) For a preliminary examination, the X-rays from the small fraction of charge states higher than 25^+ were neglected. Since their energies are higher they do not add any intensity to L_{A1}.

(ii) Neither yrast nor direct decays from high-n states can make any constant-in-time contribution to L_{A1}. Such a constant, amounting to 50% of the strength at later observation times, was in evidence and must be attributed to another source. It was therefore subtracted from L_{A1} for the present purpose.

(iii) Summing the power-law part of L_{A1} (beyond 1·6 ns) and L_{A23} allowed comparison with the Monte Carlo calculations and led to the intensity scale factor B_s per 25^+ ion and population index β_s in equations (9) and (10).

(iv) The intensities of L_{A23} and L_B, which have the same power-law at all distances, were used to fix the E2 : E1 multipole ratio.

(v) The observed intensity of L_C was reduced by subtracting from it that amount (up to 3% of L_C) which was predicted to be associated with the statistical distribution used for (iii) and (iv) above.

(vi) The amount of low-l 'direct' population, equations (2) and (8) with index β_d, which fitted the residual L_C was estimated for the two possible cases of $l = 0$ and 2.

At this point an iteration process was called for because the low-l population responsible for direct components contributed about 1% and 5% to L_{A1} and L_B respectively. Predicted amounts were duly subtracted and steps (iii) to (vi) above repeated. With such small corrections a single iteration was adequate. The results of these fits were:

(ii) L_{A1} contains a constant decay rate of 0·07% per ns per 25^+ ion.

(iii) The bulk of L_{A1} and L_{A23} is due to a statistical population with $\beta_s = 2 \cdot 135$ in 78% of cases *relative to the 25⁺ ion beam intensity.*

(iv) The E2 branch fraction is $6 \cdot 1\%$; this is an average value weighted mainly by transitions involving the 4f level. Its magnitude is reasonable (cf. Bethe and Salpeter 1957; p. 283).

(v), (vi) 97% of L_C comes from a direct decay cascade with $\beta_d = 2 \cdot 38$ and intensity $3 \cdot 6\%$ if $l = 0$, or $4 \cdot 7\%$ if $l = 2$, relative to the 25^+ ion beam.

As seen below, a more detailed consideration of the separate L_{A1} and L_{A23} groups led to a revision of the deduced fractions of ions in Rydberg states. This is chiefly because of (i) above, the neglect of the 26^+ charge fraction; nevertheless, the analysis as described above was an essential step for starting a comprehensive fitting procedure.

(b) Inclusion of 26^+ Fraction and Fitting of L_{A1} Intensity

As concluded in Section 3, L_{A1} comprises chiefly blocked yrast decays characterised by β_s. For a complete description it was necessary to assume decay lifetimes for the $\Delta n = 0$ transitions 3d to 3p and 3p to 3s. Bates–Darmgaard type calculations (Sobel'man 1972) indicated that these would be in the region of 10 to 100 ps. Acceptable fits to the data were found for combinations of τ_{3pd} and τ_{3ps} (Table 1) such as 90 and 1, 80 and 30, 60 and 60 ps, as indicated in Fig. 2.

The next stage was to take into account that the relative intensities of the statistical components of L_{A1} and L_{A23} were not consistent with the expected 25^+ trapping fraction $F^{25} = 0 \cdot 7$; any reasonable fit required a value nearer $0 \cdot 6$* in the Monte Carlo calculation. This discrepancy can be resolved by looking at the empirical method used in Part II to split the broad L_A group of lines, in conjunction with the higher X-ray energies from the 26^+ ions. Numerical decomposition of the group needed *three* gaussian components equally spaced by 127 eV. The 3s–3d level spacing, 110 ± 20 eV, is similar to the energy difference between corresponding transitions in ions with one and two L vacancies. The L_A components may now be identified as follows: L_{A1} is trapped yrast decays from 25^+, L_{A2} is a sum of untrapped yrast from 25^+ and trapped yrast from 26^+, while L_{A3} is untrapped yrast from 26^+ ions.

In order to give a complete description of all decays, it was necessary to recognise the contributions from both 25^+ and 26^+ charge states, namely background (b), statistical (s), and direct (d). These may be defined by the intensities listed in Table 2. In addition it was necessary to include not only the transitions shown in Fig. 1, but also all those allowed by the rules of Table 1. These include trapping, collapse and E2 transitions. The only way these could be accounted for was by recourse to a complete Monte Carlo treatment to predict how the decays from both charge fractions would finish up in each of the four X-ray lines at each of the 23 times of observation. We therefore had to solve 92 simultaneous linear equations representing a combination of two sequences, one for each charge state, of the steps in Section 4*a*. This was done by using a least-squares optimisation procedure for matching the observed decay curves to separate Monte Carlo spectra calculated from statistical (s) and direct (d)

* The value $F^{25} = 0 \cdot 7$ predicted in Section 3*b* corresponds to unpolarised substates of the 3d electron feeding the one vacancy of the charge 26 core. For fully polarised 3d electrons in substates $|m_l| = 0, 1, 2$ and X-rays detected at 45°, it can be shown that F would be 2/3, 5/8 and 7/8 respectively.

distributions using the basic parameters β_s, β_d, F and the E2 : E1 multipole ratio. Twelve different combinations of these were tested by evaluating a 'global' chi-squared function based on the counting statistics of both the observations and the predictions. The set which minimised this function was chosen. Thus, we obtained values for the parameters, and their probable errors, which best represent the initial intensities of the Rydberg distributions.

Table 2. Parameters used in fitting all X-ray decay curves, their definitions and their deduced values

Errors shown are normal 50% confidence levels. Trapping fractions are not included in the list of parameters, since the ones appropriate to unpolarised systems were assumed, namely $F^{25} = 7/10$ and $F^{26} = 7/15$

(a) Parameters estimated prior to Monte Carlo calculations

Parameter	Definition	Estimated from	Final value
β_d	Eqs (2, 8)	I_C decay	$2 \cdot 38 \pm 0 \cdot 04$
β_s	Eqs (2, 6, 9)	I_{A23} decay	$2 \cdot 135 \pm 0 \cdot 035$
(τ_{3dp}, τ_{3ps})	Table 1	I_{A1} decay	(90, 1), (80, 30), (60, 60) ps
E2	E2 : E1 int. ratio	$I_B : I_{A23}$ decay	$0 \cdot 061 \pm 0 \cdot 002$

(b) Additional parameters included in 'global' least-squares fit

Parameter	Definition	Value
$I_A^{25}(b)$	Background 25^+ intensity	$(0 \cdot 069 \pm 0 \cdot 004)\%$ per ns per 25^+ ion
$I_A^{26}(b)$	Background 26^+ intensity	$(0^{+0 \cdot 005}_{-0 \cdot 000})\%$ per ns per 26^+ ion
$I^{25}(s)$	Statistical 25^+ intensity	$(63 \pm 2)\%$ per 25^+ ion
$I^{26}(s)$	Statistical 26^+ intensity	$(63 \pm 2)\%$ per 26^+ ion
$I^{25}(d)$	Direct 25^+ intensity	$(2 \cdot 5 \pm 0 \cdot 3)\%$ per 25^+ ion
$I^{26}(d)$	Direct 26^+ intensity	$(2 \cdot 5 \pm 0 \cdot 3)\%$ per 26^+ ion
$\phi^{26} : \phi^{25}$	Rydberg charge-state ratio	$0 \cdot 215 \pm 0 \cdot 015$

The principal parameters involved in the fitting procedure are listed in Table 2. The fits are compared with the data in Figs 2 and 3, and are all satisfactory. In these fits trapping of 3d electrons due to angular momentum mismatch leads to 3d–3p–3s transitions with an effective lifetime of 90 ps. It should be emphasised that the trapping fractions $F^{25} = 7/10$ and $F^{26} = 7/15$ were chosen corresponding to unpolarised substate distributions (cf. the footnote on the previous page).

The main results of allowing for the minor higher charge-state fraction ϕ^{26} are to reduce the initial estimate of the proportion of ions in statistically populated Rydberg states from 78% to 63%, and to reduce the direct population from $3 \cdot 6\%$ to $2 \cdot 5\%$ (if $l = 0$) or from $4 \cdot 7\%$ to $3 \cdot 3\%$ (if $l = 2$).

5. Discussion

The main contributions to the beam–foil L X-radiation, namely L_{A1}, L_{A23} and L_B, come from 63% of the ions which have an L vacancy in a statistically populated electron distribution represented by equation (9) with $\beta_s = 2 \cdot 135$. To this must be added some 3% of ions in a non-statistical population (equation 2) with $\beta_d = 2 \cdot 38$ which is responsible for the L_C group, a total of 66% Rydberg electrons per 25^+ ion.

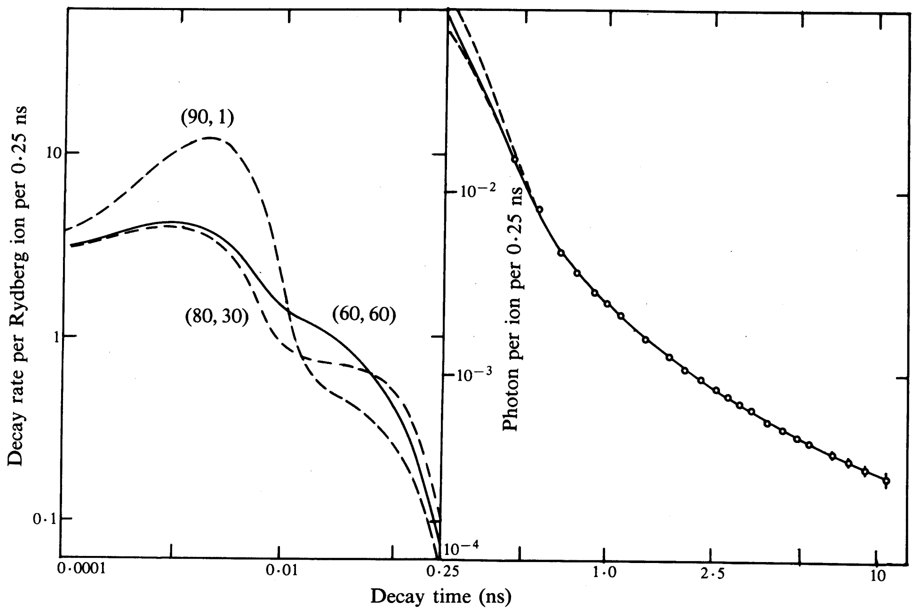

Fig. 2. On the *right* is a log–log plot of the decay of the A_1 X-ray observed in 0·25 ns time intervals downstream of a carbon target of 20 μg cm^{-2} bombarded by 130 MeV Br ions incident in a 10^+ charge state. The fitted curves use the parameters listed in Table 2. The different choices (τ_{3dp}, τ_{3ps}) are as labelled (in ps) on the *left*, which shows the calculated A_1 decay rate at short times from a statistical population. The effects of different choices of (τ_{3dp}, τ_{3ps}) are illustrated.

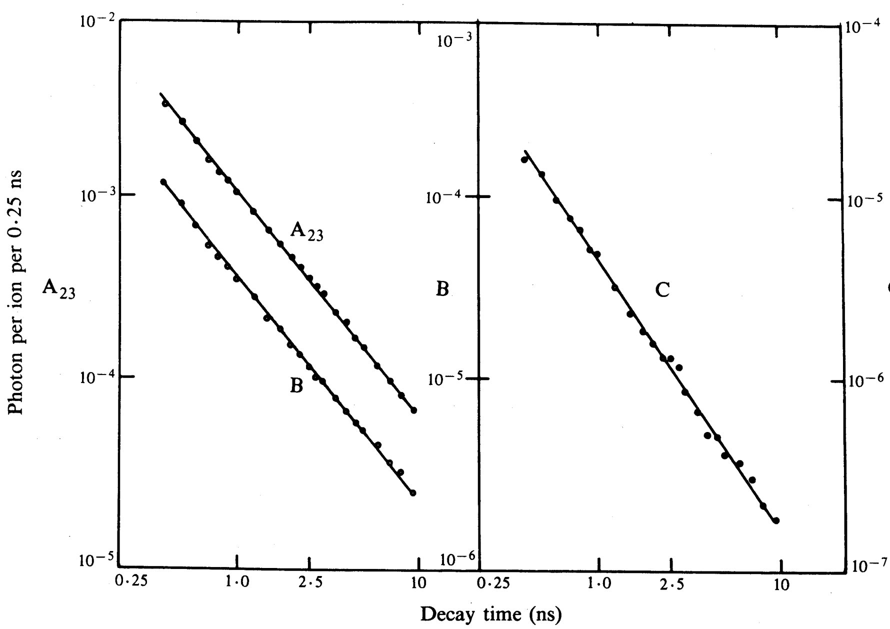

Fig. 3. On the *left* are the decays of A_{23} and B X-rays under the same conditions as in Fig. 2. The fitted lines have the same slope, corresponding to their common source in the yrast cascade. On the *right* is the decay of the C X-ray under the same conditions. The fitted line, corresponding to direct decays, is steeper than that of the yrast lines.

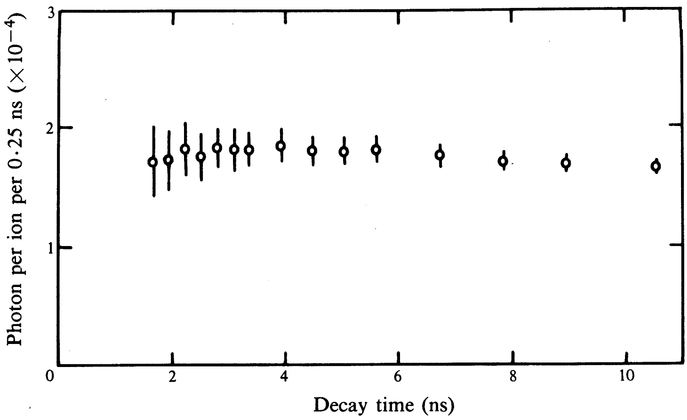

Fig. 4. Fitted background feed I_{25}(b) deduced from fits to the data of Fig. 2. At longer times the accuracy increases, leading to an asymptotic limit of $(0\cdot069\pm0\cdot004)$% per ns per 25^+ ion, in accordance with Table 2.

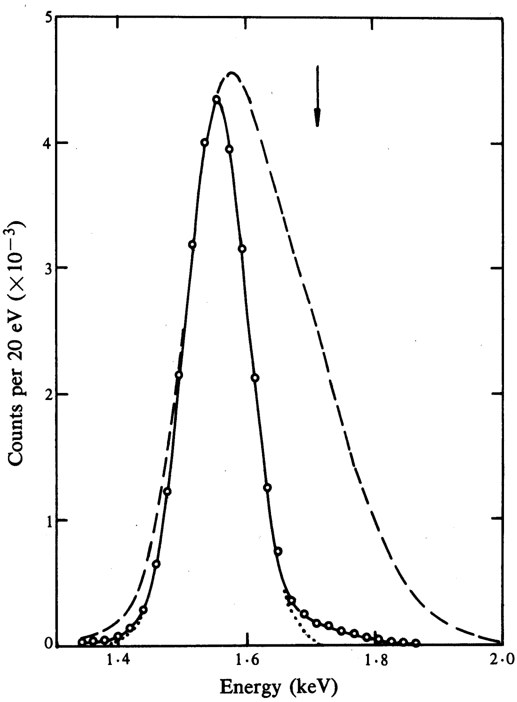

Fig. 5. Data points (joined by the solid curve) of the L X-ray spectrum observed at 64 ns decay time. The dotted curve is a Si(Li) line shape; the excess data are, at low energies, due to M X-rays, and at high energies, due to A_{23}. The dashed curve represents a spectrum at 1·68 ns decay time, reduced by the scale factor of 7·0 predicted for A_1. The relative intensities of the A_{23} line (arrowed) in the two spectra are in accordance with its decay curve.

In addition to the two initial populations thus inferred, there is a background 'feeding' the 3s level at 0·069% per ns per 25^+ ion over the range of observed times 0·4 to 10 ns. This background appears to be absent for 26^+ ions, although reasonable fits could be obtained with such a background of up to 0·005% per ns per 26^+ ion.

There is no evidence to suggest that the 26^+ charge state, with two L vacancies, has different amounts of Rydberg states or different population indices. The fitted charge-state ratio $\phi^{26} : \phi^{25}$ of $0\cdot215\pm0\cdot015$ for Rydberg ions is virtually the same as the value $0 \cdot 22 \pm 0 \cdot 02$ for all ions measured with a target of the same thickness. This is in agreement with the observations in Part I concerning the similarity of charge-state fractions and the proportions of yrast intensities in ultraviolet radiation near $n = 20$ from Fe, Ni and Cu ions.

The following unexpected results were noted:

Statistical population (63% per ion). This has a β_s value of $2 \cdot 14$, i.e. well below the 'uniform'—or OBK—value of 3. The highest value permitted by the data is $2 \cdot 26$, which would be attained by using the analytical theory either with equations (6) and (9) and assuming 'instant collapse', or by assuming an initial population of yrast states only.

Direct population ($2 \cdot 5$% per ion). From the decay of L_C one deduces a low-l (0 or 2) population comparable with that due to the statistical one. If the direct and statistical populations are attributed to distributions in accordance with equations (2) and (9) with $l = 0$, and summed over all $n \geqslant 3$, it follows that the direct population is 70% of the $l = 0$ component of the statistical population.

Background ($0 \cdot 069$% per ns per 25^+ ion). The 3s state appears to be repopulated as the ion proceeds downstream after foil excitation. No obvious mechanism exists for such a continuous feeding in the decay time range $0 \cdot 45$ to $10 \cdot 7$ ns. The presence of such a background in X-rays from decay of the 3s level, and its apparent absence from all other decays, is quite remarkable. That it is accurately established is illustrated in Fig. 4, in which the amount of L_{A1} predicted from the Monte Carlo method, consistent with all other X-ray decay curves, has been subtracted from the observed L_{A1} intensity. The residual constant feed as observed 64 ns ($1 \cdot 14$ m) after traversal of the target is shown in Fig. 5, together with a spectrum taken at $1 \cdot 68$ ns scaled down according to the predicted decay of L_{A1}. Thus, the L_{A1} background was in evidence long after any mechanism involving delayed capture of convoy electrons could be expected to occur.

There is no experimental evidence on whether all or any of these three distinct populations are fed by charge exchange with bound electrons (direct capture), with free electrons (radiative capture), or from some rearrangement within the ion. The very large fraction (66% per ion) of Rydberg states we have observed must be noted. This value includes contributions from all n values of the deduced distributions from $n = 3$ upwards. For our actual observation times between $0 \cdot 45$ and $10 \cdot 7$ ns, the cascades would be dominated by decays from states with n values between 20 and 40 (from 'pure' yrast) to between 50 and 135 (from direct decay), with 'collapse' filling in the range between. Throughout this paper we have assumed that power-law decays are evidence for constant population indices, and there is no obvious physical reason to suggest that either population should be truncated for the low n values from which most of the intensity originates. It is worth noting that if the populated fraction of 66% Rydberg states per ion were to be quoted per core (26^+) state it would well exceed 100%, so the concept that electrons 'settle' on cores, as assumed for example by Dybdal *et al.* (1986), cannot be used: rather a major rearrangement of charge states at or after foil exit must be invoked. The extent to which this involves free and bound electrons is unknown. Evidently there is a need for the use of external fields as probes, as has been done for example by Kanter *et al.* (1985), to help solve these problems.

References

Bashkin, S., and Stoner, J. O. (1975, 1976, 1981). 'Atomic Energy Levels and Grotrian Diagrams', Vols 1–3 (North-Holland: New York).

Bethe, H. A., and Salpeter, E. E. (1957). 'Quantum Mechanics of One and Two Electron Atoms' (Springer: Berlin).

Betz, H.-D., Röschenthaler, D., and Rothermel, J. (1983). *Phys. Rev. Lett.* **50**, 34.

Betz, H.-D., Rothermel, J., and Bell, F. (1980). *Nucl. Instrum. Methods* **170**, 243.

Betz, H.-D., Rothermel, J., Röschenthaler, D., Bell, F., Schuch, R., and Nolte, G. (1982). *Phys. Lett.* A **91**, 12.

Dybdal, K., Sorensen, J., Hvelplund, P., and Knudsen, H. (1986). *Nucl. Instrum. Methods* B **13**, 581.

Hasse, R. W., Betz, H.-D., and Bell, F. (1979). *J. Phys.* B **12**, L711.

Hay, H. J., Newton, C. S., and Treacy, P. B. (1983). *Aust. J. Phys.* **36**, 7.

Hay, H. J., Pender, L. F., and Treacy, P. B. (1986). *Aust. J. Phys.* **39**, 15.

Kanter, E. P., Koenig, W., Faibis, A., and Zabransky, B. J. (1985). *Nucl. Instrum. Methods* B **10/11**, 36.

Omidvar, K. (1975). *Phys. Rev.* A **12**, 911.

Rothermel, J., Betz, H.-D., Bell, F., and Zacek, V. (1982). *Nucl. Instrum. Methods* **194**, 341.

Sobel'man, I. I. (1972). 'Introduction to the Theory of Atomic Spectra' (Pergamon: Oxford).

Manuscript received 10 September, accepted 20 November 1986